# Chapter 4

# Observable to Study the Underlying Event and Existing Tune

The underlying events UE are all the processes not associated with the primary hard scatter in an hadron-hadron collision.
All the process described in the previous section: ISR, FSR, MPI, and BBR and their interactions with color exchanges, contribute to the Underlying Event (UE) in the proton-proton collision.
As an example, in a proton-proton collision with a $Z$ boson production, that then can decay in two leptons ($l^+$ and $l^-$) and in the end these two leptons observed by the experiment, we have that the hard scattering is represented from the scatters between the two partons that generate the $Z$ boson. While, the so called UE is represented from all the extra scatterings, the various radiations and in general all the activity not associated with this primary hard scattering.

It is important to underline the fact that most of the observables to study the UE are sensible only to the sum of these contributions and not to the single ones. So, a good description of all these processes and their interplay is really important in order to study the complexes finals states originating from this scatters that contribute to the observables.
In this chapter these observables sensible to the UE are introduced and described with more detail.

## 4.1 Minimum Bias Measurements and Underlying Event topology

A Minimum Bias (MB) measurement is a collection of inelastic events with a loose event selection. Which means the events are collected requiring the minimal interaction with the detector (the smallest possible bias). The most of the interactions in MB observation are soft, $p_T \lesssim 2$ GeV, but the study of the UE requires at least one hard scattering ($p_T \gtrsim 2$ GeV) presence; in fact the UE is given by the underlying activity to a primary hard scatter.
To study the UE the topological structure of an hadron-hadron collision is used. The analysis is performed on an *event-by-event* basis. In the analysis the direction of the leading object is used to define regions in the $\eta - \phi$ space. Where $\eta$ is the

pseudorapidity defined as $\eta = -\log\tan\left(\frac{\theta}{2}\right)$, while $\phi$ is the azimuthal angle in the $x-y$ plane. The last one is defined from the direction of the leading object as $\Delta\phi = \phi - \phi_{\text{leading}}$ .

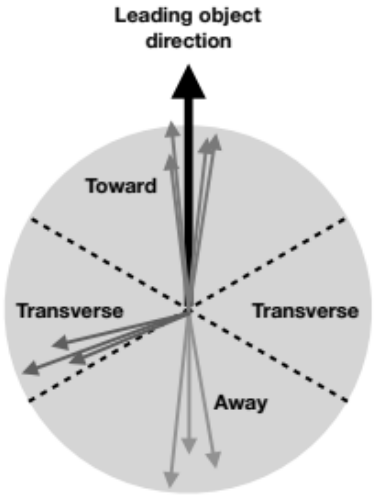


| Region | Angular region |
|---|---|
| Toward | $\lvert\Delta\phi\rvert < 60°$ |
| Away | $60° < \Delta\phi < 120°$ |
| Transverse | $\lvert\Delta\phi\rvert > 120°$ |

**Figure 4.1:** This figure shows the four regions for the description of the UE on a event-by-event analysis. The angular values, defining the four regions, are shown in the table. The regions are defined starting from the leading object direction. The toward and away regions contain most of the contribution from the hard scattering (e.g. in a $t\bar{t}$ production event the two quark $t$ are located in these regions); while, the transverse region are the ones in between the two other regions, these are the most important for the study of the UE.

The regions classification is shown in Fig. 4.1, we have:

- **Toward region**: the region that contains the leading object, this region contains the most of the particles produced by the hard interaction.
- **Away region**: this region contains the objects that recoil against the leading object, also this region contains mostly the particles produced by the hard interaction.
- **Transverse regions**: the two transverse regions are the most sensitive to UE.

The toward and away regions are the ones with the major contribution from the primary hard scattering, in fact in a dijets event the leading jet is expected in the toward region while the next-to-leading jet in the away region.
The two transverse regions are called:

  - **TransMAX**: This is the transverse region that contains the *maximum* number of charged particles, or scalar $p_T$ sum of charged particles. This regions includes both MPI and hard-process contamination. As an example, in events with 3-jets production these region can contains the extra jet.
  - **TransMIN**: is the transverse region that contains the *minimum* number of charged particles, or scalar-$p_T$ sum of charged particles. This region is the most sensitive to MPI effects.

The leading object definition depend on the type of event under observation and defer from one analysis to another. The charged-particle with largest $p_T$ [29], the dilepton system in Drell-Yan observation [30, 31] or $t\bar{t}$ events [32] can all be used as leading object in the analyses for the UE event.
So we are interest in studying the transMAX and transMIN regions in particular the observable sensitive to UE in these regions. The main observables studied in these regions are: the charged-particle density and the charged-particle scalar-$p_T$ sum density in the $\eta - \phi$ space.

In an hadron-hadron collision with two jets productions it is observed that not only the toward and away regions activity increases with the hardness of the collision ($p_T^{max}$) but also the transverse regions activity increases with it. This is shown in Fig. 4.2, where the different color lines refer to different scales for the collision. It is observed that the away region ($60 \leq |\Delta\phi| \leq 120$) at increasing energy for the collision become broader this is related to the increasing quantity of FSR.
This increment in the transverse regions activity cannot be explained only by the increase of the FSR. To explain this rise one need to attribute activity in the transverse regions to MPI: the number of extra scatters increases with energy. This rise is related to the density functions for the partons inside the hadrons that increse when probed at higher energies and so the partons become denser packed in hadrons. In this way the extra scatters probability is larger to higher energies.

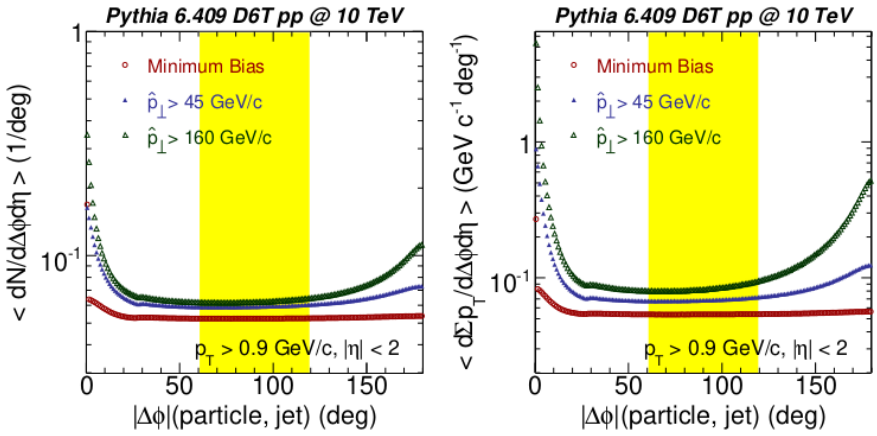


**Figure 4.2:** A comparison between three different scales for the interaction, in PYTHIA. The multiplicity of charged particles (left) and the scalar-$p_T$ sum of charged particles (right) are simulated. The activity in the transverse regions increase due two effects: the FSR this is related to the broadening of the away region so some events from the shower end up in the transverse region (yellow band) but this alone can't explain the increment so is required the introduction of the MPI in the description. Figure from chapter 5 of [33].

The evolution of these two quantities in transMAX region as a function of the transverse-momentum of the leading object (measurement of the energy scale for the collision) is shown in more detail in Fig. 4.3. The two distributions show a rapid raise at low leading-object $p_T$ than a very low rise starts.

Now we want to look for the sensitivity of these observables to some PYTHIA8 parameters. In figure Fig. 4.4 is shown the effect of the MPI on booth the distributions shown before separately for TransMAX and TransMIN regions. The figure

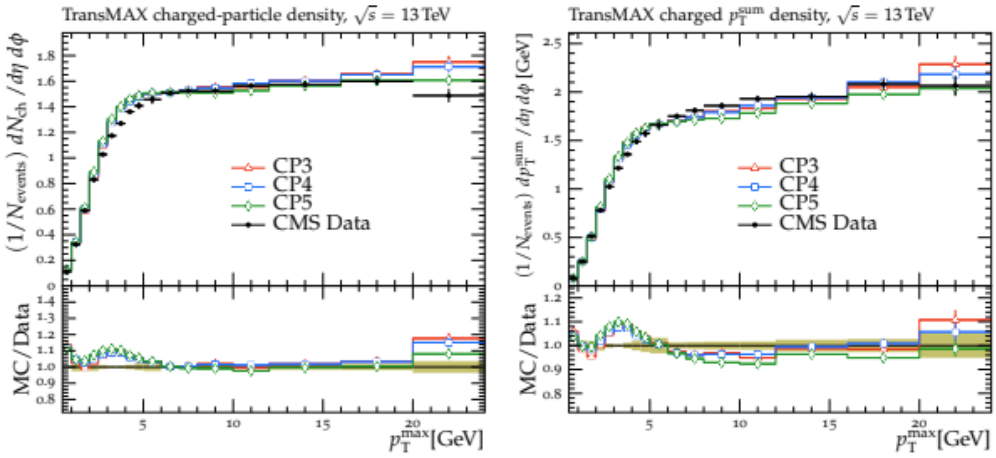


**Figure 4.3:** The evolution of the charged-particles density (left) and of the scalar-$p_T$ sum density of charged particles (right) as a function of the energy scale for the scattering (leading object $p_T$), the two distribution increase quite rapidly in the first bins than they saturate ($\approx 6-7$ GeV) the scalar-$p_T$ sum density increase a little bit more, for $p_T >$ but very slowly. The black dots are the experimental point and are compared to prediction with CMS PYTHIA tunes: CP3, CP4 and CP5; they are described with more details in the next chapter. Figure from [34].

shows the case with MPI (red line) and the case when the MPI are switched off (blue line). As expected the MPI are needed to explain the activity in the transverse regions. When the MPI are switched-on the number of particle produced is higher than the case when they are off. From this figure is clear that MPI are the main contribution in the activity of these TransMAX and TransMIN regions. It's obviously that the discrepancy increases as the hard scale of the interaction increases, in fact in low $p_T$ regions the $p_T$ evolution start at a lower value so the phase-space, for the extra collisions to occur, is smaller.

Another important observation that was also pointed out in the Chapter 3.1 is that the amount of activity in the two transverse regions is also dependent on the center-of-mass energy. This evolution is shown in Fig. 4.5 for two different energy. The amount of MPI increase with $\sqrt{s}$ that was expected from the evolution of the PDF with the energy of the collision: the hadrons become denser-packed when probed to higher energies. In Fig. 4.5 the charged particle density and the scalar sum of the transverse momentum in the transverse regions data are compared for two different center-of-mass energies. The data are also compared to existing different CMS tuning.

So these observables are the main ones we are going to use in our tune and used in previous tunes for the UE. The data from the activity in the TransMAX and TransMIN regions have been collected by a large number of experiment at different center-of-mass energies.

### 4.1.1 Observables in Z production processes

In the last part of this work we are going to tune the primordial $k_T$ another important parameter in the simulation of hadron-hadron collisions. An unresolved question is that the primordial $k_T$ value required for the description of the observed cross section for the Z production is very large respect to the expected value derived from the

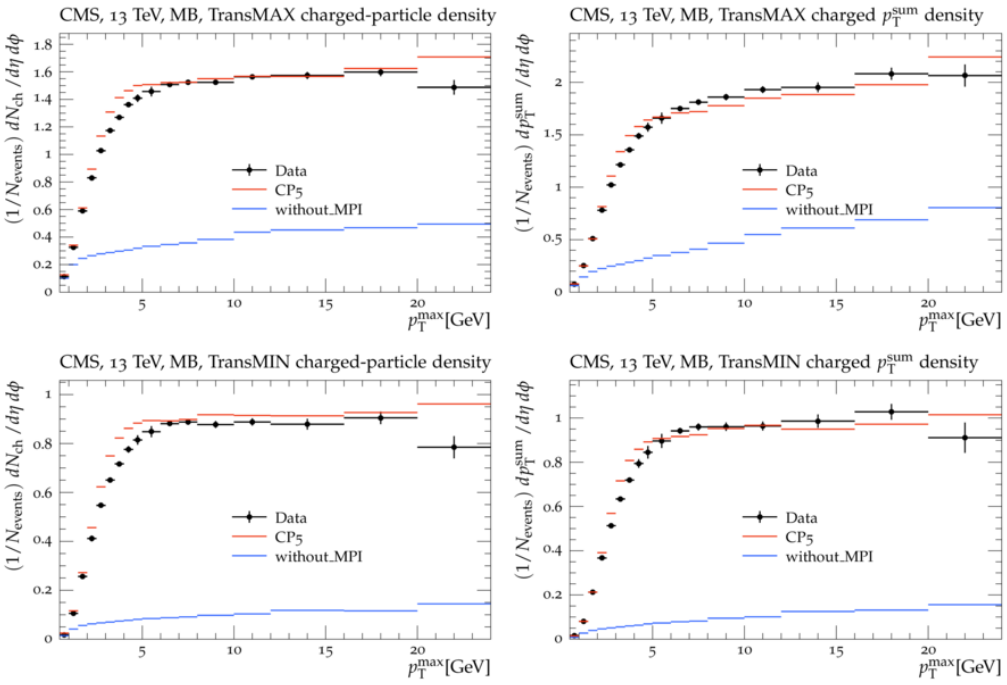


**Figure 4.4:** This image shows the effect of the MPI in the transMAX and TransMin regions. The contribution of the parton shower alone can't explain the contributions of the underlying event in these two regions (blue line) the introduction of the contribution from the MPI is necessary (red line). The two simulations are compared to the data from [29].

typical size of an hadron in Eq. 3.29. This very high value is not understood by first principles so it is required a tune of this parameter in the Monte Carlo generator in order to describe the data in a good way.
The observables to study the primordial $k_T$ are the differential cross section for Z production in proton-proton collision in Drell-Yan observation as a function of the transverse momentum of the Z boson (Fig. 4.7 left) and as a function of the $\phi^*_\eta$ angle (Fig. 4.7 right). Where the angle $\phi^*_\eta$ is defined as:

$$\phi^*_\eta = \tan\left(\frac{\pi - \Delta\phi}{2}\right) \sin(\theta^*_\eta) \quad , \tag{4.1}$$

where $\Delta\phi$ is the azimuthal angle between the two leptons. The angle $\theta^*_\eta$ instead is the angle measured respect to the beam direction in the rest frame of the dilepton system (frame with leptons emitted back-to-back), so is defined as:

$$\cos(\theta^*_\eta) = \tanh\left(\frac{\eta^- - \eta^+}{2}\right) \quad , \tag{4.2}$$

with $\eta^+$ and $\eta^-$ the pseudorapidities of the two leptons [35].

To full simulate the Z production spectrum we have to merge matrix element calculation and space shower to do this we used the FxFx merging scheme that have been introduced in Chapter 2. As shown in Fig. 4.7 the description with out FxFx is good only in the first bins. The strategy we follow for the tuning of the primordial kT is tu tune the Primordial $k_T$ in this low region. From these two distribution we

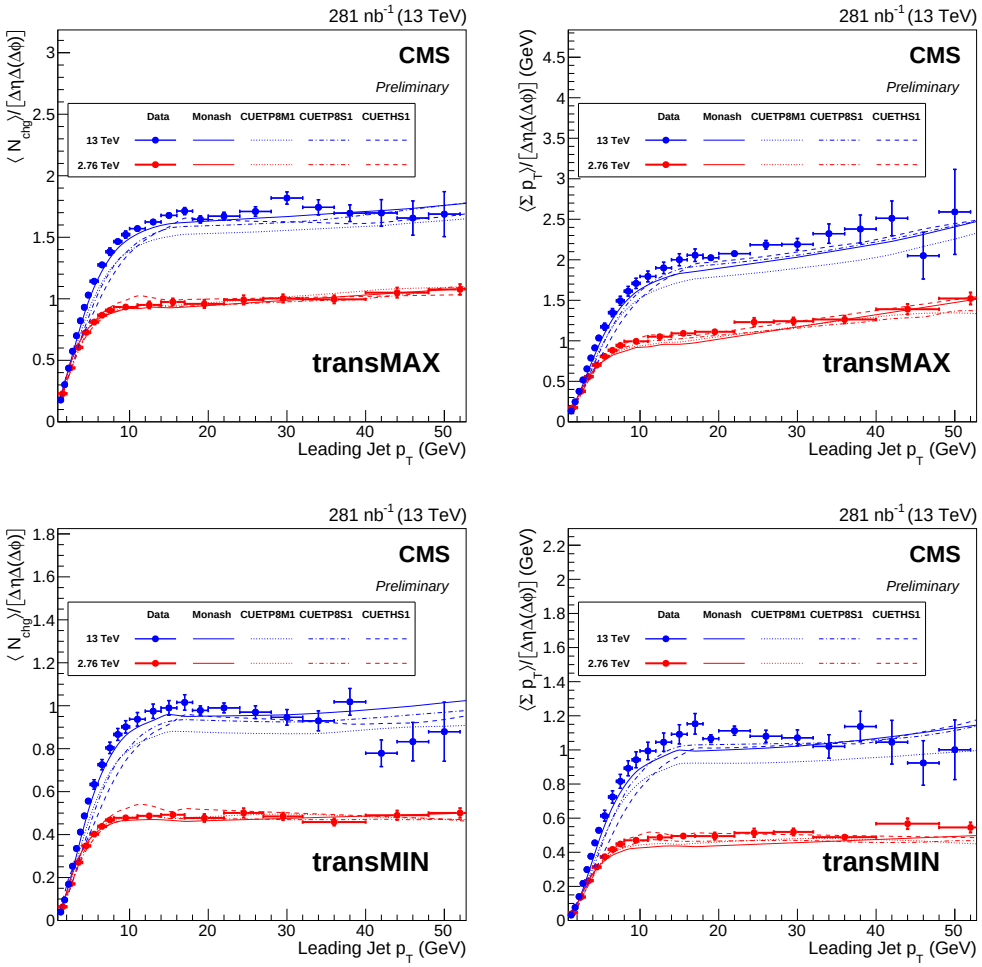


**Figure 4.5:** The charged particle density in the transMAX (upper left) and transMIN (lower left) regions and of the charged particle $p_T$-sum in the transMAX (upper right) and the transMIN (lower right) regions evolution as function of the center-of-mass energy is shown. The red ones are the data for $\sqrt{s} = 2.76$ and the blue ones for $\sqrt{s} = 13$ and these are compare to different CMS tunes. Figure from [29]

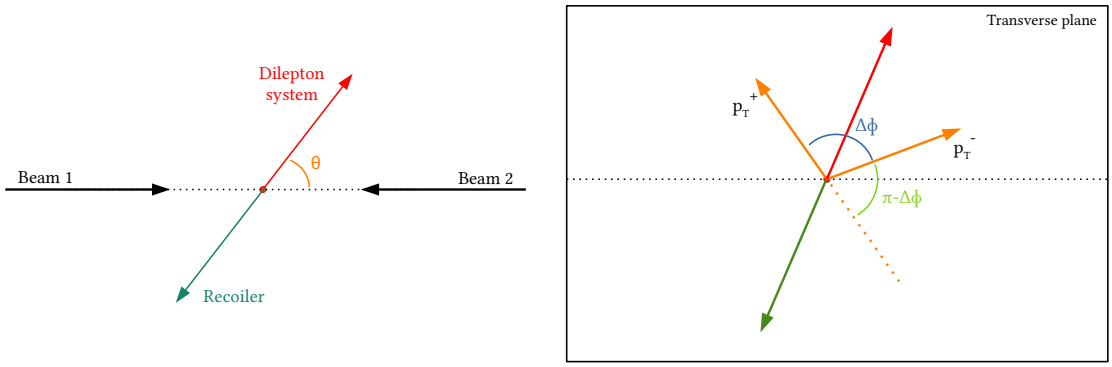


**Figure 4.6:** A schematic representation of a Drell-Yan observation with a description of the angles used in the definition of $\phi^*_\eta$ in Eq. 4.1.

take only the first 5 bins each.
Than we are going to run the FxFx only for the comparison once the parameters are tuned. This is going to be discussed in Chapter 7 where we perform the primordial

$k_T$ tune.

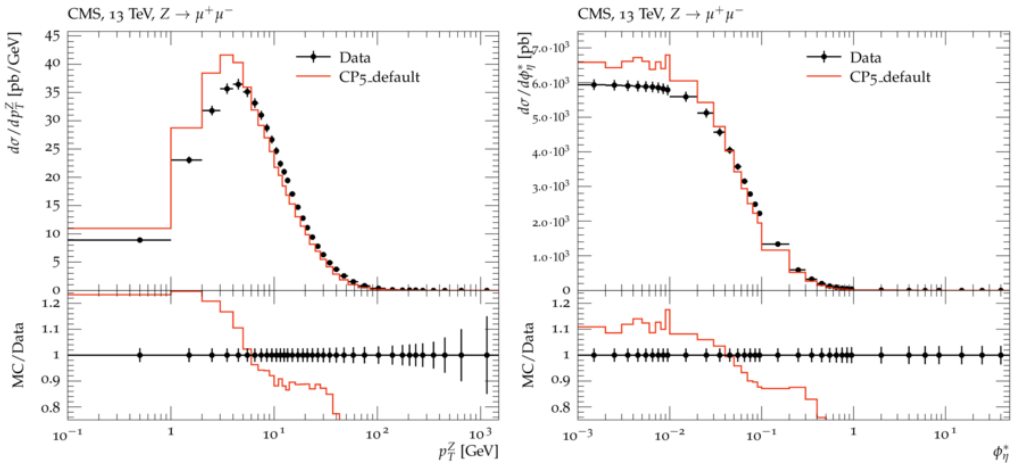


**Figure 4.7:** Here are shown the distribution, from the [36] CMS analysis at $\sqrt{s} =$ 13 TeV, that we are going to use for the tune of the primordial $k_T$. The left one is the $Z$ boson production cross section as a function of the transverse momentum of the $Z$ boson. On the right the differential cross section for the $Z$ boson production as a function of the $\phi_\eta^*$ angle. The red line is the the PYTHIA8 description before the tune of the primordial $k_T$ and without the FxFx merging scheme so only the first bins have to be taken into account.

In the following section we will introduce the existing CMS tunes for the minimum bias and UE. These tunes are able to reproduce very well the observables described in Section 4.1 at 1.96, 7 and 13 TeV. But as we are going to see in Chapter 2 the tunes do not describe well the low region of the $Z$ boson production cross section so a further tune on these observable is performed.

## 4.2 Previous Tune for the Underlying Event

In the paper [34] the CMS collaboration presents new PYTHIA8 tunes for the underlying event (UE). The tunes are called CP and a number from 1 to 5 where CP stands for "CMS PYTHIA8". The tunes are performed changing the values of the coupling constant $\alpha_s$ for the ISR, FSR, hard scattering and MPI and changing the order of the evolution for the $\alpha_s$ with the $Q^2$ value of the interaction. Another difference among these tunes is the choice of the PDF set: CP1 and CP2 use a LO PDF, CP3 a NLO one, while CP4 and CP5 tunes use a NNLO PDF set.

The tuned parameters are shown in Table 4.1 with the associated variation ranges and a recall on the definition of each one.

| Parameter description | Name in PYTHIA8 | Range considered |
|---|---|---|
| MPI threshold [GeV], `pT0Ref`, at $\sqrt{s} = \sqrt{s_0}$ | `MultipartonInteractions:pT0Ref` | $1.0 - 3.0$ |
| Exponent of $\sqrt{s}$ dependence, $\epsilon$ | `MultipartonInteractions:ecmPow` | $0.0 - 0.3$ |
| Matter fraction contained in the core | `MultipartonInteractions:coreFraction` | $0.1 - 0.95$ |
| Radius of the core | `MultipartonInteractions:coreRadius` | $0.1 - 0.8$ |
| Range of color reconnection probability | `ColorReconnection:range` | $1.0 - 9.0$ |

**Table 4.1:** This table report the five parameters tuned for the UE and Minimum Bias in CP* tunes, the variation ranges used for the sampling are shown in the last column. Table from [34]

These parameters are the ones that govern the number of MPI and the amount of Color Reconnections[1]. These CP* tunes want to be a general (multi-purpose) tunes for UE and minimum bias observables described above.

These tunes are performed with the standard tool for the high energy physics tune: PROFESSOR.

### 4.2.1 The distributions used for the Tune

The observables distributions used for the tune are the following ones:

- The pseudorapidity distribution of charged hadrons ($p$, $K$ ,$\pi$) measured for an inclusive selection in inelastic proton-proton collisions [37];
- Charged particle density and charged particle scalar $p_T^{sum}$ in TransMIN and TransMAX regions at different $\sqrt{s}$ (1.96 TeV [38], 7 TeV [39], 13 TeV [29]);
- The pseudorapidity distributions for single diffractive (SD) and non single diffractive (NSD) events selection [40].

In the next chapter we will describe our tune using `mcnntunes` and in it we used the same distribution listed here. All the graphs for these observables are then shown with the final tunes descriptions.

### 4.2.2 Pyhtia configuration and the tunes

On the top section of Table 4.2 and Table 4.3 are reported the values for the `pythia8` parameters used in the CP tunes and, on the bottom, the five parameters resulting from the tune.
Below we are going to focus on CP5 tune. We are going to reproduce this tune using the same settings for `pythia8` but using a different tuning software: `mcnntunes`.

Next chapter discusses the general approaches to the tune and why we use machine learning and and on the description of the main tool used for the tuning in this work MCNNTUNES.

[1]Note that the parameters related to the simulation of the hadronization and beam remnant are set to the values of the Monash tune

| PYTHIA8 parameter | CP1 | CP2 |
|---|---|---|
| PDF Set | NNPDF3.1 LO | NNPDF3.1 LO |
| $\alpha_S(m_Z)$ | 0.130 | 0.130 |
| `SpaceShower:rapidityOrder` | off | off |
| `MultipartonInteractions:EcmRef` [GeV] | 7000 | 7000 |
| $\alpha_S^{\mathrm{ISR}}(m_Z)$ value/order | 0.1365/LO | 0.130/LO |
| $\alpha_S^{\mathrm{FSR}}(m_Z)$ value/order | 0.1365/LO | 0.130/LO |
| $\alpha_S^{\mathrm{MPI}}(m_Z)$ value/order | 0.130/LO | 0.130/LO |
| $\alpha_S^{\mathrm{ME}}(m_Z)$ value/order | 0.130/LO | 0.130/LO |
| `MultipartonInteractions:pT0Ref` [GeV] | 2.4 | 2.3 |
| `MultipartonInteractions:ecmPow` | 0.15 | 0.14 |
| `MultipartonInteractions:coreRadius` | 0.54 | 0.38 |
| `MultipartonInteractions:coreFraction` | 0.68 | 0.33 |
| `ColorReconnection:range` | 2.63 | 2.32 |

**Table 4.2:** CP1 and CP2 tunes settings are report here together with the values for the parameters tuned. CP1 and CP2 use a LO PDF set. CP1 $\alpha_s$ is different between matrix element calculation and MPI that use a value of 0.1365 ISR and FSR that instead use 0.130. While, CP2 use the same value for all processes, it is fixed at 0.130. In both cases $\alpha_s$ run with a LO evolution. Table from [34]

| PYTHIA8 parameter | CP3 | CP4 | CP5 |
|---|---|---|---|
| PDF Set | NNPDF3.1 NLO | NNPDF3.1 NNLO | NNPDF3.1 NNLO |
| $\alpha_S(m_Z)$ | 0.118 | 0.118 | 0.118 |
| `SpaceShower:rapidityOrder` | off | off | on |
| `MultipartonInteractions:EcmRef` [GeV] | 7000 | 7000 | 7000 |
| $\alpha_S^{\mathrm{ISR}}(m_Z)$ value/order | 0.118/NLO | 0.118/NLO | 0.118/NLO |
| $\alpha_S^{\mathrm{FSR}}(m_Z)$ value/order | 0.118/NLO | 0.118/NLO | 0.118/NLO |
| $\alpha_S^{\mathrm{MPI}}(m_Z)$ value/order | 0.118/NLO | 0.118/NLO | 0.118/NLO |
| $\alpha_S^{\mathrm{ME}}(m_Z)$ value/order | 0.118/NLO | 0.118/NLO | 0.118/NLO |
| `MultipartonInteractions:pT0Ref` [GeV] | 1.52 | 1.48 | 1.41 |
| `MultipartonInteractions:ecmPow` | 0.02 | 0.02 | 0.03 |
| `MultipartonInteractions:coreRadius` | 0.54 | 0.60 | 0.76 |
| `MultipartonInteractions:coreFraction` | 0.39 | 0.30 | 0.63 |
| `ColorReconnection:range` | 4.73 | 5.61 | 5.18 |

**Table 4.3:** here are reported CP3, CP4 and CP5 tunes settings, and the results for the tune. The three tunes use an equal $\alpha_s$ value for al the processes, $\alpha_s = 0.118$ running with a NLO evolution. The difference between CP3 and the other two tune is that CP3 use a NLO PDF set while CP4 and CP5 a NNLO one. CP5 ISR emission is also ordered according to rapidity. Table from [34]

# Bibliography


[1] Steven Weinberg. A model of leptons, Nov 1967. URL https://link.aps.org/doi/10.1103/PhysRevLett.19.1264.

[2] J. D. Bjorken. Asymptotic Sum Rules at Infinite Momentum. *Phys. Rev.*, 179: 1547–1553, 1969. doi: 10.1103/PhysRev.179.1547.

[3] Sidney D Drell and Tung-Mow Yan. Partons and their applications at high energies, 1971. ISSN 0003-4916. URL https://www.sciencedirect.com/science/article/pii/0003491671900716.

[4] J M Campbell, J W Huston, and W J Stirling. Hard interactions of quarks and gluons: a primer for lhc physics, Dec 2006. ISSN 1361-6633. URL http://dx.doi.org/10.1088/0034-4885/70/1/R02.

[5] L N Lipatov. The parton model and perturbation theory, 1975. URL http://cds.cern.ch/record/400357.

[6] Vladimir Naumovich Gribov and L N Lipatov. Deep inelastic ep scattering in perturbation theory, 1972. URL https://cds.cern.ch/record/427157.

[7] G. Altarelli and G. Parisi. Asymptotic freedom in parton language, 1977. ISSN 0550-3213. URL https://www.sciencedirect.com/science/article/pii/0550321377903844.

[8] Yuri L. Dokshitzer. Calculation of the Structure Functions for Deep Inelastic Scattering and e+ e- Annihilation by Perturbation Theory in Quantum Chromodynamics., 1977.

[9] W.J. Stirling. private communication. URL http://www.hep.ph.ic.ac.uk/~wstirlin/plots/plots.html.

[10] F. Bloch and A. Nordsieck. Note on the radiation field of the electron, Jul 1937. URL https://link.aps.org/doi/10.1103/PhysRev.52.54.

[11] Toichiro Kinoshita. Mass singularities of feynman amplitudes, 1962. URL https://doi.org/10.1063/1.1724268.

[12] T. D. Lee and M. Nauenberg. Degenerate systems and mass singularities, Mar 1964. URL https://link.aps.org/doi/10.1103/PhysRev.133.B1549.

[13] A. Kulesza, G. Sterman, and W. Vogelsang. Electroweak vector boson production in joint resummation, 2002. URL https://arxiv.org/abs/hep-ph/0207148.

[14] Torbjörn Sjöstrand, Stefan Ask, Jesper R. Christiansen, Richard Corke, Nishita Desai, Philip Ilten, Stephen Mrenna, Stefan Prestel, Christine O. Rasmussen, and Peter Z. Skands. An introduction to pythia 8.2, Jun 2015. ISSN 0010-4655. URL http://dx.doi.org/10.1016/j.cpc.2015.01.024.

[15] Manuel Bähr, Stefan Gieseke, Martyn A. Gigg, David Grellscheid, Keith Hamilton, Oluseyi Latunde-Dada, Simon Plätzer, Peter Richardson, Michael H. Seymour, Alexander Sherstnev, and Bryan R. Webber. Herwig++ physics and manual, Nov 2008. ISSN 1434-6052. URL http://dx.doi.org/10.1140/epjc/s10052-008-0798-9.

[16] T Gleisberg, S Hoeche, F Krauss, A Schaelicke, S Schumann, and J Winter. Sherpa 1. , a proof-of-concept version, Feb 2004. ISSN 1029-8479. URL http://dx.doi.org/10.1088/1126-6708/2004/02/056.

[17] E. Boos, M. Dobbs, W. Giele, I. Hinchliffe, J. Huston, V. Ilyin, J. Kanzaki, K. Kato, Y. Kurihara, L. Lonnblad, M. Mangano, S. Mrenna, F. Paige, E. Richter-Was, M. Seymour, T. Sjostrand, B. Webber, and D. Zeppenfeld. Generic user process interface for event generators, 2001.

[18] Stefano Catani, Frank Krauss, Bryan R Webber, and Ralf Kuhn. Qcd matrix elements + parton showers. *Journal of High Energy Physics*, 2001(11):063–063, Nov 2001. ISSN 1029-8479. doi: 10.1088/1126-6708/2001/11/063. URL http://dx.doi.org/10.1088/1126-6708/2001/11/063.

[19] Stefano Frixione and Bryan R Webber. Matching nlo qcd computations and parton shower simulations. *Journal of High Energy Physics*, 2002(06):029–029, Jun 2002. ISSN 1029-8479. doi: 10.1088/1126-6708/2002/06/029. URL http://dx.doi.org/10.1088/1126-6708/2002/06/029.

[20] Stefano Frixione, Paolo Nason, and Bryan R Webber. Matching nlo qcd and parton showers in heavy flavour production. *Journal of High Energy Physics*, 2003(08):007–007, Aug 2003. ISSN 1029-8479. doi: 10.1088/1126-6708/2003/08/007. URL http://dx.doi.org/10.1088/1126-6708/2003/08/007.

[21] Stefano Frixione and Bryan R. Webber. The mc@nlo 3.1 event generator, 2005.

[22] Rikkert Frederix and Stefano Frixione. Merging meets matching in MC@NLO. *JHEP*, 12:061, 2012. doi: 10.1007/JHEP12(2012)061.

[23] Victor S. Fadin. BFKL resummation. *Nucl. Phys. A*, 666:155–164, 2000. doi: 10.1016/S0375-9474(00)00022-1.

[24] I. I. Balitsky and L. N. Lipatov. The Pomeranchuk Singularity in Quantum Chromodynamics. *Sov. J. Nucl. Phys.*, 28:822–829, 1978.

[25] Richard D. Ball, Valerio Bertone, Stefano Carrazza, Luigi Del Debbio, Stefano Forte, Patrick Groth-Merrild, Alberto Guffanti, Nathan P. Hartland, Zahari Kassabov, José I. Latorre, Emanuele R. Nocera, Juan Rojo, Luca Rottoli,

Emma Slade, and Maria Ubiali. Parton distributions from high-precision collider data. *The European Physical Journal C*, 77(10), Oct 2017. ISSN 1434-6052. doi: 10.1140/epjc/s10052-017-5199-5. URL http://dx.doi.org/10.1140/epjc/s10052-017-5199-5.

[26] FRANK SIEGERT. Monte-carlo event generation for the lhc, 2010. URL http://etheses.dur.ac.uk/484/.

[27] B. Andersson, G. Gustafson, G. Ingelman, and T. Sjöstrand. Parton fragmentation and string dynamics. *Physics Reports*, 97(2):31–145, 1983. ISSN 0370-1573. doi: https://doi.org/10.1016/0370-1573(83)90080-7. URL https://www.sciencedirect.com/science/article/pii/0370157383900807.

[28] Torbjorn Sjostrand. Jet Fragmentation of Nearby Partons. *Nucl. Phys. B*, 248: 469–502, 1984. doi: 10.1016/0550-3213(84)90607-2.

[29] Underlying Event Measurements with Leading Particles and Jets in pp collisions at $\sqrt{s} = 13$ TeV. Technical report, CERN, Geneva, 2015. URL https://cds.cern.ch/record/2104473.

[30] Serguei Chatrchyan et al. Measurement of the underlying event in the Drell-Yan process in proton-proton collisions at $\sqrt{s} = 7$ TeV. *Eur. Phys. J. C*, 72: 2080, 2012. doi: 10.1140/epjc/s10052-012-2080-4.

[31] A. M. Sirunyan et al. Measurement of the underlying event activity in inclusive Z boson production in proton-proton collisions at $\sqrt{s} = 13$ TeV. *JHEP*, 07:032, 2018. doi: 10.1007/JHEP07(2018)032.

[32] Albert M. Sirunyan et al. Study of the underlying event in top quark pair production in pp collisions at 13 TeV. *Eur. Phys. J. C*, 79(2):123, 2019. doi: 10.1140/epjc/s10052-019-6620-z.

[33] Florian Bechtel. *The underlying event in proton-proton collisions*. PhD thesis, Hamburg U., 2009.

[34] Albert M Sirunyan et al. Extraction and validation of a new set of CMS PYTHIA8 tunes from underlying-event measurements. *Eur. Phys. J. C*, 80(1):4, 2020. doi: 10.1140/epjc/s10052-019-7499-4.

[35] A. Banfi, S. Redford, M. Vesterinen, P. Waller, and T. R. Wyatt. Optimisation of variables for studying dilepton transverse momentum distributions at hadron colliders. *Eur. Phys. J. C*, 71:1600, 2011. doi: 10.1140/epjc/s10052-011-1600-y.

[36] Albert M Sirunyan et al. Measurements of differential Z boson production cross sections in proton-proton collisions at $\sqrt{s} = 13$ TeV. *JHEP*, 12:061, 2019. doi: 10.1007/JHEP12(2019)061.

[37] Vardan Khachatryan et al. Pseudorapidity distribution of charged hadrons in proton-proton collisions at $\sqrt{s} = 13$ TeV. *Phys. Lett. B*, 751:143–163, 2015. doi: 10.1016/j.physletb.2015.10.004.

[38] Timo Antero Aaltonen et al. Study of the energy dependence of the underlying event in proton-antiproton collisions. *Phys. Rev. D*, 92(9):092009, 2015. doi: 10.1103/PhysRevD.92.092009.

[39] Measurement of the Underlying Event Activity at the LHC at 7 TeV and Comparison with 0.9 TeV. Technical report, CERN, Geneva, 2012. URL http://cds.cern.ch/record/1478982.

[40] Albert M. Sirunyan et al. Measurement of charged particle spectra in minimum-bias events from proton–proton collisions at $\sqrt{s} = 13\,\text{TeV}$. *Eur. Phys. J. C*, 78 (9):697, 2018. doi: 10.1140/epjc/s10052-018-6144-y.

[41] Andy Buckley, Hendrik Hoeth, Heiko Lacker, Holger Schulz, and Jan Eike von Seggern. Systematic event generator tuning for the LHC. *Eur. Phys. J. C*, 65: 331–357, 2010. doi: 10.1140/epjc/s10052-009-1196-7.

[42] Stefano Carrazza and Marco Lazzarin. N3pdf/mcnntunes: mcnntunes 0.1.0, October 2020. URL https://doi.org/10.5281/zenodo.4071125.

[43] Marco Lazzarin, Simone Alioli, and Stefano Carrazza. MCNNTUNES: Tuning Shower Monte Carlo generators with machine learning. *Comput. Phys. Commun.*, 263:107908, 2021. doi: 10.1016/j.cpc.2021.107908.

[44] Martín Abadi, Ashish Agarwal, Paul Barham, Eugene Brevdo, Zhifeng Chen, Craig Citro, Greg S. Corrado, Andy Davis, Jeffrey Dean, Matthieu Devin, Sanjay Ghemawat, Ian Goodfellow, Andrew Harp, Geoffrey Irving, Michael Isard, Yangqing Jia, Rafal Jozefowicz, Lukasz Kaiser, Manjunath Kudlur, Josh Levenberg, Dandelion Mané, Rajat Monga, Sherry Moore, Derek Murray, Chris Olah, Mike Schuster, Jonathon Shlens, Benoit Steiner, Ilya Sutskever, Kunal Talwar, Paul Tucker, Vincent Vanhoucke, Vijay Vasudevan, Fernanda Viégas, Oriol Vinyals, Pete Warden, Martin Wattenberg, Martin Wicke, Yuan Yu, and Xiaoqiang Zheng. TensorFlow: Large-scale machine learning on heterogeneous systems, 2015. URL https://www.tensorflow.org/. Software available from tensorflow.org.

[45] F. Rosenblatt. The perceptron: A probabilistic model for information storage and organization in the brain. 1958. URL https://doi.org/10.1037/h0042519.

[46] Kurt Hornik. Approximation capabilities of multilayer feedforward networks. *Neural Networks*, 4(2):251–257, 1991. ISSN 0893-6080. doi: https://doi.org/10.1016/0893-6080(91)90009-T. URL https://www.sciencedirect.com/science/article/pii/089360809190009T.

[47] Moshe Leshno, Vladimir Ya. Lin, Allan Pinkus, and Shimon Schocken. Multilayer feedforward networks with a nonpolynomial activation function can approximate any function. *Neural Networks*, 6(6):861–867, 1993. ISSN 0893-6080. doi: https://doi.org/10.1016/S0893-6080(05)80131-5. URL https://www.sciencedirect.com/science/article/pii/S0893608005801315.

[48] Nikolaus Hansen. The CMA evolution strategy: A tutorial. *CoRR*, abs/1604.00772, 2016. URL http://arxiv.org/abs/1604.00772.

[49] G. Cowan. *Statistical data analysis*. Oxford University Press, USA, 1998.

[50] Richard D. Ball et al. Parton distributions from high-precision collider data. *Eur. Phys. J. C*, 77(10):663, 2017. doi: 10.1140/epjc/s10052-017-5199-5.

[51] Albert M Sirunyan et al. Measurement of differential cross sections for Z boson production in association with jets in proton-proton collisions at $\sqrt{s} = 13$ TeV. *Eur. Phys. J. C*, 78(11):965, 2018. doi: 10.1140/epjc/s10052-018-6373-0.